Thermodynamic Characterization of the Interaction Behavior of a Hydrophobically Modified Polyelectrolyte and Oppositely Charged Surfactants in Aqueous Solution: Effect of Surfactant Alkyl Chain Length

Guangyue Bai,[†] Marieta Nichifor,[‡,§] António Lopes,[‡] and Margarida Bastos*[,†]

CIQ (UP), Department of Chemistry, Faculty of Sciences, University of Porto, R. Campo Alegre, 687, P-4169-007 Porto, Portugal, Instituto de Tecnologia Química e Biológica (ITQB/UNL), P-2781-901 Oeiras, Portugal, and "Petru Poni" Institute of Macromolecular Chemistry, Iasi, Romania

Received: August 2, 2004; In Final Form: October 8, 2004

We have used a precision isothermal titration microcalorimeter (ITC) to measure the enthalpy curves for the interaction of a hydrophobically modified polyelectrolyte (D40OCT30) with oppositely charged surfactants (SC_nS) in aqueous solution. D40OCT30 is a newly synthesized polymer based on dextran having pendant *N*-(2-hydroxypropyl)-*N*,*N*-dimethyl-*N*-octylammonium chloride groups randomly distributed along the polymer backbone with degree of substitution of 28.1%. The employed anionic surfactants are sodium octyl sulfate (SC_8S) and sodium tetradecyl sulfate ($SC_{14}S$). Microcalorimetric results along with turbidity and kinematic viscosity measurements demonstrate systematically the thermodynamic characterization of the interaction of D40OCT30/SC_nS. A three-dimensional diagram with the derived phase boundaries is drawn to describe the effect of the alkyl chain length of surfactant and of the ratio between surfactant and pendant groups on the interaction. A more complete picture of the interaction mechanism for D40OCT30/SC_nS systems is proposed here.

Introduction

Compared to the well-known behavior of uncharged polymer/ionic surfactant systems, oppositely charged polyelectrolyte/surfactant (PES) systems often present unusual physicochemical characteristics. The inherent structural features of polyelectrolytes and surfactants are crucial factors leading to the intricate behaviors and rich self-assembly morphologies of PES mixtures in aqueous solution. The change of polyelectrolyte molecular structure is usually based on the introduction of ionic or hydrophobic moieties on environmentally friendly nonionic polymer or polyelectrolyte precursors, which induces a significant influence on the solution behavior of PES mixtures. From the early studies on relatively hydrophilic polyelectrolytes such as sodium dextran sulfate (NaDxS) and sodium poly(styrenesulfonate) (NaPS),[1−3] poly(methacrylic acid) (PMA),[4] or sodium hyaluronate (NaHy)[5−7] to the hydrophobically modified polyelectrolytes (HMPE), research in the field of polyelectrolyte−surfactant interactions has made impressive progress. Iliopoulos et al.[8] and Petit-Agnely et al.[9] have systematically investigated the interaction of hydrophobically modified sodium polyacrylate with cationic surfactant. Guillemet and Piculell[10] provided a detailed explanation for the interesting phase behavior that occurs in the system of a hydrophobically modified cationic cellulose derivative and an anionic surfactant (SDS). Kabanov's group[11,12] synthesized a novel type of self-assembly material, poly(ethylene oxide)-*b*-poly(sodium methacrylate) (PEO-*b*-PMA), that can spontaneously form vesicles with the surfactant ionic groups under condition of electroneutrality, while regular PES complexes usually precipitate. All these systems have a strong tendency to self-associate and/or to associate with surfactants, forming spontaneously hydrophobic cores in aqueous solution, exhibiting a great potential in drug/gene delivery research and in other biomedical applications.

In the reported studies of these PES systems, the most commonly studied surfactants have been the conventional anionic sodium alkyl sulfates (SC_nS) and cationic alkyltrimethylammonium bromide/chloride (C_nTAB or C_nTACl). These surfactants alter substantially some key characteristics of the PES solutions making the systems suitable for different studies, such as viscosity, surface tension, phase behavior, and morphology. In particular, when the alkyl chain length of surfactant changes, the behavior of the PES solution often presents a great variation.[3−5,13−19] More recently, increasing interest has been directed toward the supramolecular structure of PES complexes that are spontaneously formed in many systems. Zhou et al.[16,17] have investigated the nanostructures of polyelectrolyte−surfactant complexes between linear poly(vinylamine hydrochloride) chains and oppositely charged SC_nS by small-angle X-ray scattering, in which a surfactant induces a structural transition that has been found to depend on hydrocarbon tail length.

So far two main fruitful views have emerged from the extensive studies of PES complexes: (i) The critical aggregation concentration (cac) at which the surfactant begins to bind to the polyelectrolyte is much lower than the critical micelle concentration (cmc) of the surfactant, and increases with increasing polyelectrolyte concentration. This is in contrast to the behavior for uncharged polymer/surfactant system, where the cac decreases only slightly and is only weakly dependent on the polymer concentration. (ii) An associative phase separation takes place, which is the most obvious feature of PES mixtures. In general, a single phase appears at low and high

* To whom correspondence should be addressed. Fax: +351-22-6082959. E-mail: mbastos@fc.up.pt.
† University of Porto.
‡ ITQB/UNL.
§ "Petru Poni" Institute of Macromolecular Chemistry.

10.1021/jp046552b CCC: $30.25
Published on Web 12/02/2004

surfactant concentrations, and close to charge neutralization concentration (cnc) a phase separation occurs.[5−8,10,20−22] Detailed studies on the phase behavior of different PES systems have opened the way to a better understanding of polyelectrolyte/surfactant interactions.[23]

A widely accepted model for the interaction between polyelectrolyte and surfactant is that the surfactant molecules are adsorbed to the polyelectrolyte chains as micelle-like aggregates—the "necklace of beads" model.[5,8] Moreover, the association between polyion and surfactant can be considered as an ion-exchange process, in which polyion counterions are replaced by bound surfactant molecules.[24,25] Recently Hansson[23] proposed a thermodynamic model (cell model) where the interaction is viewed as a result from the binding of polyion chains to the surface of oppositely charged surfactant micelles. The model includes the free energy contributions to the system at the cac and explains some previously found phenomena, such as the correlation between the cac and the aggregation number, as well as the dependence of the cac on the polyelectrolyte concentration. However, these models cannot account for all particular interaction patterns that we have found in our PES systems. The solution behavior of PES systems strongly depends on their composition, i.e., on the molar ratio of surfactant to polyion unit (n_s/n_p).[10,18,26,27] The mixed system often goes through a series of more complicated association processes as n_s/n_p increases: the formation of PES complexes, micellization, precipitation, and redissolution of the PES complexes. Furthermore, the mechanisms of these association processes depend to a great extent on changes of headgroup size, charge, and tail group structure of the surfactant. Therefore, a full explanation for these phenomena is still a matter of debate and deserves further study.

Our previous study[28] and a few other reports[14,29−32] have shown that isothermal titration calorimetry (ITC) is an ideal technique to investigate the interactions between polyelectrolyte and surfactant. In comparison with viscosity[8,33] and fluorescence[9,34] that often are used, the distinct advantages of ITC are the direct energy measurement and the wider allowed concentration range. As a result, both the energetic information and accurate concentration boundaries for the description of phase behavior are derived simultaneously. In our recent study on the interactions of a newly hydrophobically modified plyelectrolyte (D40OCT30) with SDS,[28] it has been learned that D40OCT30 with the pendant *N*-(2-hydroxypropyl)-*N*,*N*-dimethyl-*N*-octylammonium chloride groups randomly distributed along the polymer backbone can self-associate into intra- or intermolecular micelle-like clusters, in the studied concentration range. The added SDS molecules strongly associate with D40OCT30 due to attractive hydrophobic and electrostatic interactions between SDS and the pendant groups of the polyelectrolyte. Thus the critical concentrations corresponding to each association process (mixed micellization, coacervation and redissolution, etc.) were determined by ITC, combined with conductivity and turbidity measurements. The work presented here follows from the previous one. We will report a systematic study on systems of D40OCT30/sodium alkyl sulfates (SC$_n$S), performed mainly by ITC, combined with kinematic viscosity and UV−vis spectrophotometry measurements. The two anionic surfactants of sodium alkyl sulfates were the ones with 8 and 14 carbon atoms in the alkyl chain (denoted as SC$_8$S and SC$_{14}$S, respectively). Our goal is to determine the effect of the alkyl chain length of surfactant on PES interaction, and to try to elucidate the mechanism of such interaction.

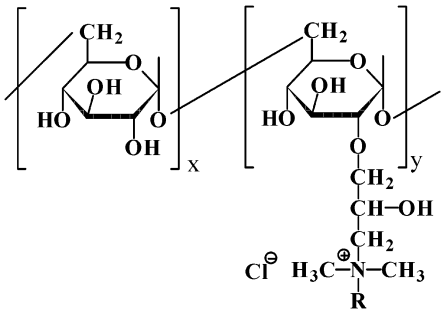

Figure 1. Chemical structure of the cationic polyelectrolyte (D40OCT30) obtained by chemical modification of dextran (R = $CH_3(CH_2)_7$; DS = 28.1 mol %).

Experimental Methods

Materials. The studied polyelectrolyte (D40OCT30) belongs to a series of cationic polysaccharides we are synthesizing, with pendant quaternary ammonium groups, as shown in Figure 1, where y is the degree of hydrophobic modification, $100[y/(x + y)]$ mol %. It was synthesized by chemical modification of a dextran sample (Sicomed S.A., Bucharest) with molar mass M_w = 40 000 and M_w/M_n = 1.12, as determined by capillary viscometry and static light scattering in aqueous solution. The polyelectrolyte molecule D40OCT30 contains a degree of substitution of 28% (of amino groups carrying an octyl chain) and therefore has 69.4 positive charges per polymer chain. The detailed procedure for the synthesis of these polymers has been described in our previous paper.[28]

The anionic surfactants (SC$_n$S), sodium octyl sulfate (SC$_8$S) (Merck, 99.0%), and sodium tetradecyl sulfate (SC$_{14}$S) (Research Chemical Ltd., 99%), were used without further purification. All the solutions were prepared using water produced by a Milli-Q filtration system, either by weight or by volume, and were stabilized at room temperature for 2 days before use.

Isothermal Titration Microcalorimetry (ITC). The microcalorimeter unit used in this work and the experimental procedure have been described in detail in our previous work.[28] All experiments were performed at 308.15 ± 0.01 K. Briefly, the calorimetric titration experiments consisted of a series of consecutive additions of concentrated surfactant solution into water or concentrated surfactant + polymer solutions into polymer solution. The reason to have polymer in the syringe was to maintain a constant polymer concentration, necessary for building the 3-D diagram that shows the phase boundaries for the different mixtures. The volume of polymer solution or water in the calorimetric vessel was 2.6 mL. The titrating solution was automatically added in aliquots of 4.16−8.32 μL from a modified gastight Hamilton syringe, through a thin stainless steel capillary, until the desired range of concentration had been covered. Each titration run was repeated at least three times.

Turbidity Measurements. The turbidity of D40OCT30/SC$_n$S solutions was measured on an 845x UV−vis spectrophotometer, at a wavelength of 400 nm in a quartz sample cell with a light path of 10 mm, thermostated at 308.15 K with a water bath (Julabo, F25-HP). The concentrations of surfactant and D40OCT30 solutions were the same as those used for the ITC experiments. The measured values were corrected with the polymer-free blank, and were only recorded after the value became stable (about 2−3 min).

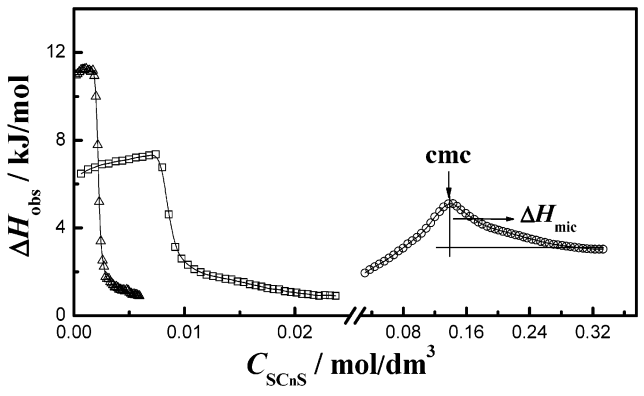

Figure 2. Microcalorimetric titration curves for dilution of concentrated SC_8S, $C = 2$ mol/dm^3 (○), $SC_{12}S$, $C = 0.2$ mol/dm^3 (□), and $SC_{14}S$, $C = 0.05$ mol/dm^3 (△), into water, at 308.15 K.

Viscosity Measurements. Stock solutions of polymer and $SC_{14}S$ in water were prepared and aliquots mixed to obtain the desired concentration of both components. The obtained mixtures were stirred for 24 h at room temperature for equilibration, and then their flow time (t, in s) was determined with Ubbelohde capillary viscometers of different capillary constants (k, in mm^2/s^2). Kinematic viscosities (in cSt) were calculated as $\eta = tk$. All the measurements were performed in a thermostated bath at 308.15 ± 0.10 K.

Results and Discussion

Micellization of SC_nS in Aqueous Solution. In this study, we have used SC_nS with different length alkyl chains ($n = 8$, 12, and 14) as titrant, and therefore it is essential to measure the dilution enthalpy curves of the concentrated surfactant solution into pure water, as shown in Figure 2. The dilution process for $SC_{14}S$, $SC_{12}S$, and SC_8S is endothermic, and the values of cmc and ΔH_{mic} are determined from these curves. The thermodynamic meaning of the different parts of the surfactant dilution enthalpy curve and the methods to determine cmc and ΔH_{mic} have been described in detail in the literature.[35−37] The values that we obtained[28] for cmc and ΔH_{mic} of $SC_{12}S$ are in very good agreement with the ones reported by Wang and Olofsson.[35] The curve for the dilution of $SC_{14}S$ is similar to that of $SC_{12}S$ (Figure 2), showing in order the processes of monomer formation, partial demicellization, and dilution of the added micelles. The curve for the dilution of SC_8S differs from the ones of $SC_{14}S$ and $SC_{12}S$. Before cmc, ΔH_{obs} increases with the concentration of SC_8S, in agreement with the usual dilution pattern. At cmc, we have only partial demicellization, and after cmc the ΔH_{obs} does not change steeply as in the other two cases, but decreases gradually until about twice cmc. The broad concentration range of the micellization process suggests a large deviation from the phase separation model, and is a consequence of very weak hydrophobicity of the short alkyl chain leading to a small aggregation number for the micelle and a lower cooperativity of the micellization process.[38] Nevertheless, we use the same method to calculate ΔH_{mic} as we used for $SC_{12}S$ and $SC_{14}S$ to have a common basis for comparison of the thermodynamic parameters for the three surfactants and their interactions with the polyelectrolyte. The values of cmc, ΔH_{mic}, and related parameters of the three surfactants are given in Table 1. The cmc values are in good agreement with literature values,[36] and decrease with increasing alkyl chain length (n) of the surfactants. The micellization enthalpies are negative and the absolute value increases with increasing n, because of the stronger intermolecular hydrophobic interaction resulting from longer hydrophobic chains and of the larger aggregation numbers.

ITC Profile for D40OCT30/SC_nS Systems. Typical microcalorimetric curves for D40OCT30/SC_nS systems are presented in Figure 3, where any abrupt change in peak area always indicates a change in interaction energy. Therefore, from the change in peak area we can predict the change in solution behavior, such as a phase transition or a change in aggregate morphologies.

In the experiments with D40OCT30/$SC_{14}S$ systems we noticed the appearance of an unusual baseline drift (Figure 3b,c): for 0.10% D40OCT30 it appears for surfactant concentrations between 1.65 and 4.0 mmol/dm^3 and for 0.25% D40OCT30 it appears between 3.6 and 6.5 mmol/dm^3. We did a careful examination for the process by performing parallel experiments using the same titration unit but with a transparent cell, outside the calorimeter channel, in a thermostated bath at the same temperature. It is clear that the baseline drift occurs at the moment where the viscosity increases, and the later viscosity decrease corresponds to the moment where the calorimetric signal is back to baseline. This suggests the possibility that the baseline drift is caused by heat of friction. We confirm this possibility by turning off and on the stirring of the titration cell when the baseline drift appears, and observing that it comes back to baseline. Repeated experiments show clearly that the effect is caused by heat of friction. Such friction effect is inevitable, and we observe that it is in fact imposing for higher polymer concentrations ($C_{polymer} > 0.50\%$). Therefore, we do not present any values for polymer concentrations higher than 0.25%, as we consider that no good data treatment would produce reliable enthalpy data. For $C_{polymer} \leq 0.25\%$, the effect can be eliminated through subtracting a baseline that follows the event. We should stress that such a baseline drift phenomenon was very reproducible, which gives us a clear indication that the aggregation morphology is changing in this concentration range. This led us to do parallel measurements of kinematic viscosity, as discussed below.

Figures 4−6 show that, in the presence of D40OCT30, the observed enthalpies (ΔH_{obs}) for each injection vary with the final concentrations of $SC_{14}S$ or SC_8S in the calorimetric vessel. For D40OCT30/SC_8S systems, the ITC experiments have been performed in two surfactant concentration ranges (low and high). We observe that in the low concentration range, where the surfactant concentration in the cell is always below the cmc, after the completion of the titration experiment, no clear solution is found (Figure 5). Therefore, we increase the surfactant concentration in the syringe (2.0 mol/dm^3) so as to follow the complete interaction process (Figure 6). The corresponding dilution curves of surfactant solutions into water are included in these figures for comparison. Differences between the observed curves with and without D40OCT30 must result from polyelectrolyte−surfactant interactions or morphological change induced by the surfactant. In the beginning of the titration, all the $\Delta H_{obs}-C_{SC_nS}$ curves present exothermic ΔH_{obs} values, deviating largely from the case of pure surfactant. Further, several obvious break points emerge in each ITC curve, and eventually the curves approach the dilution curve of pure surfactant. If we compare the profile of D40OCT30/SC_8S with ones of D40OCT30/$SC_{14}S$ and D40OCT30/$SC_{12}S$,[28] the former curves have fewer breaks than the two latter ones. It has been observed that approximately the same number of break points

TABLE 1: Thermodynamic Parameters for Anionic Surfactants (SC$_n$S) in Aqueous Solution at 308.15 K

SC$_n$S	cmc[a] (mmol/dm^3)	N[b]	β[c]	ΔH_{mic} (kJ/mol)	ΔG_{mic}[d] (kJ/mol)	$-T\Delta S_{mic}$ (kJ/mol)
SC$_8$S[e]	138	27	0.66	−2.10	−8.4	−6.3
SC$_{12}$S[f]	7.78	64	0.73	−5.35	−21.5	−16.2
SC$_{14}$S[e]	1.94	80	0.81	−9.32	−29.0	−19.7

[a] The error is less than 2%. [b] Aggregation numbers from ref 39. [c] β is the effective micellar charge fraction from ref 40. [d] $\Delta G_{mic} = (1 + \beta)\,RT$ ln[cmc]. [e] Present work. [f] From our previous work (ref 28).

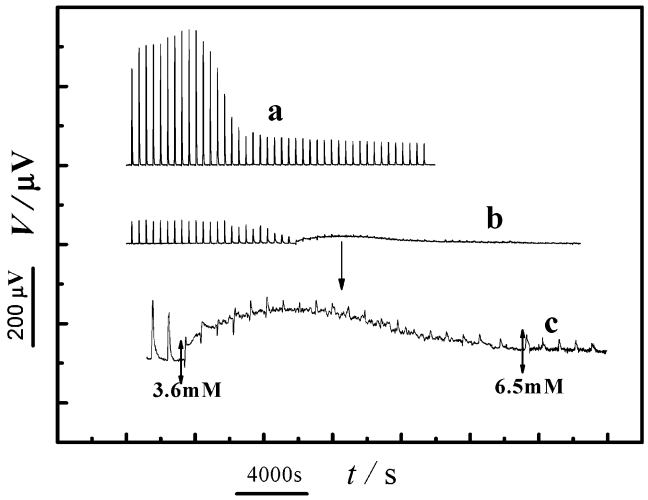

Figure 3. Typical microcalorimetric curves for titration of D40OCT30 with SC$_8$S (a) ($C_{polymer}$ = 1.0%) and with SC$_{14}$S (b) ($C_{polymer}$ = 0.25%). (c) is an enlargement of the middle part of titration curve b.

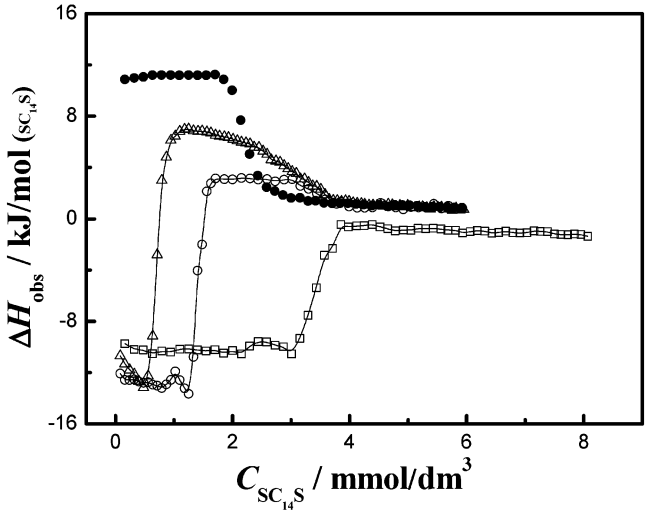

Figure 4. Observed enthalpy vs concentration of surfactant for titration of D40OCT30 with SC$_{14}$S (C = 0.05 mol/dm^3) + D40OCT30, for different concentrations of D40OCT30: (△) 0.05%; (○) 0.10%; (□) 0.25%. (●): dilution of pure surfactant in water.

is present for both SC$_{12}$S and SC$_{14}$S. As we will see in the following text, they do in some cases refer to different physical processes.

Thermodynamic Characterization of D40OCT30/SC$_n$S Systems. For D40OCT30/SC$_{14}$S systems, the characteristics of the interaction are described in detail in Figure 7, where we present the observed enthalpy curve together with the corresponding turbidity curve for a polymer concentration of 0.10%. Before the break, the negative ΔH_{obs} keeps almost constant and there is no phase separation. This exothermic effect is believed to reflect the electrostatic binding of negatively charged surfactant molecules to the grafted cationic surfactant-like side chains of the polymer, with the formation of ionic pairs and further mixed clusters. The binding curve deviates largely from

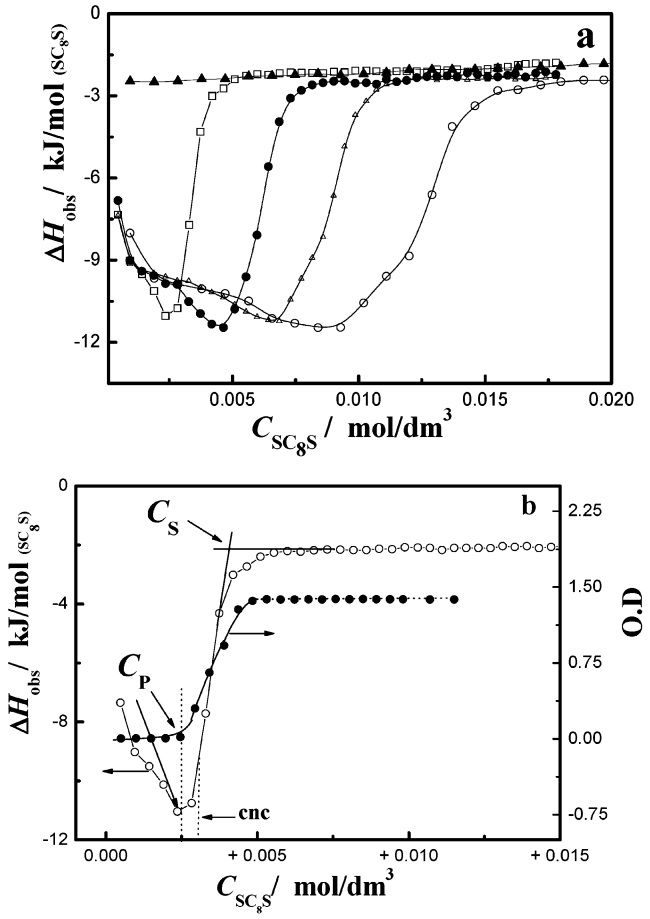

Figure 5. Observed enthalpy vs concentration of surfactant for titration of D40OCT30 with SC$_8$S + D40OCT30 in low concentration regime (C(SC$_8$S) = 0.3 mol/dm^3) (a), for different polymer concentrations of (○) 1.0%, (△) 0.75%, (●) 0.50%, and (□) 0.25%, and (▲) for dilution of pure surfactant in water. (b) (○): detail of the way to obtain C_P and C_S for 0.25% polymer concentration. (●): corresponding turbidity curve (optical dispersion, λ = 400 nm, T = 308.15 K) for the mixed solution.

the dilution curve in the absence of D40OCT30, and the results from fluorescence measurements have shown that the concentration at which binding starts (C_1) is several orders of magnitude lower than the cmc of surfactant (results to be published). We cannot obtain this critical concentration by calorimetry, due to the sensitivity limit of the calorimeter. The aggregation concentration of D40OCT30−SC$_{14}$S complex is determined from the onset point of the first break of each observed enthalpy curve (keeping the notation of our previous paper, we will call it CAC$_{complex}$). The CAC$_{complex}$ values under different polymer concentrations are listed in Table 2.

After CAC$_{complex}$, the decrease of ΔH_{obs} absolute values within a narrow concentration range indicates that the process between CAC$_{complex}$ and C_P will have a total positive enthalpy change. Therefore, this process is entropy-driven. It should be noted that in this concentration range the system becomes a little turbid but without any precipitation. At C_P, which corresponds to the beginning of a large increase in the turbidity curve (Figure 7),

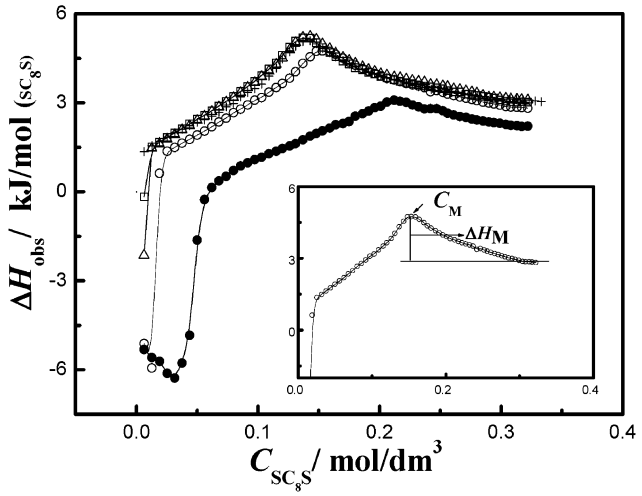

Figure 6. Observed enthalpy vs concentration of surfactant for titration of D40OCT30 with SC_8S + D40OCT30 in high concentration regime (C = 2 mol/dm^3), for different polymer concentrations: (□) 0.10%; (△) 0.25%; (○)1.0%; (●) 3.0%. (+): dilution of pure surfactant in water. The insert is an enlargement of part of the titration curve for 1.0% polymer concentration showing how we determined cmc and ΔH_M.

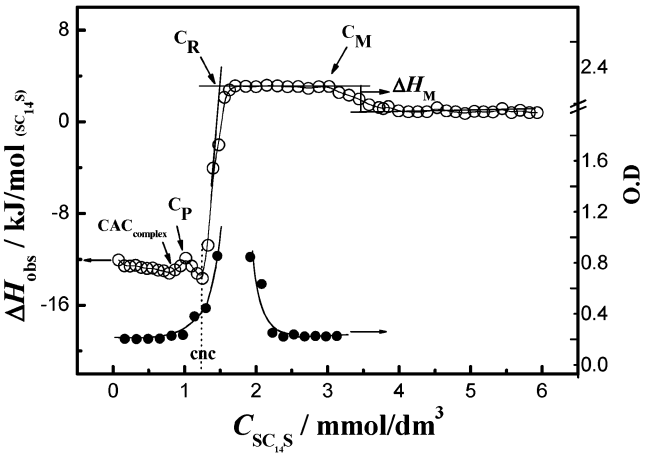

Figure 7. Plot of observed enthalpies as a function of surfactant concentration for titration of D40OCT30 (0.10%) with $SC_{14}S$ (C = 0.05 mol/dm^3) + D40OCT30 (0.10%) (○). The figure shows a detailed analysis of the curve, showing the various interaction events described in the text. The obtained turbidity curve (optical dispersion, λ = 400 nm, T = 308.15 K) for D40OCT30 (0.10%)−$SC_{14}S$ mixed solutions at the reported concentrations is also shown (●).

a clear phase separation is observed, and the new phase is a dispersion of a viscous fluid. We keep samples with this proportion of mixture after a turbidity measurement and we observe that, after several days at rest, they will precipitate as a gel-like phase on the bottom. Therefore, this concentration (C_P) is called the critical precipitation (coacervation) concentration. After C_P, an increasingly exothermic process is apparent on the enthalpy curve until the charge neutralization concentration (cnc), which corresponds to the point of maximum phase separation in the system. After the cnc, ΔH_{obs} becomes progressively less exothermic, until reaching C_R, where ΔH_{obs} tends to level off. This critical concentration (C_R) just indicates the onset of a redissolution process. Thereafter the turbidity decreases quickly, but the viscosity of the system starts to increase. This suggests that the gel forms in the concentration range between C_R and C_M. Finally, C_M can be viewed as the critical micelle concentration of SC_nS built around the polymer where the $SC_{14}S$ molecules are self-associated as micelles.

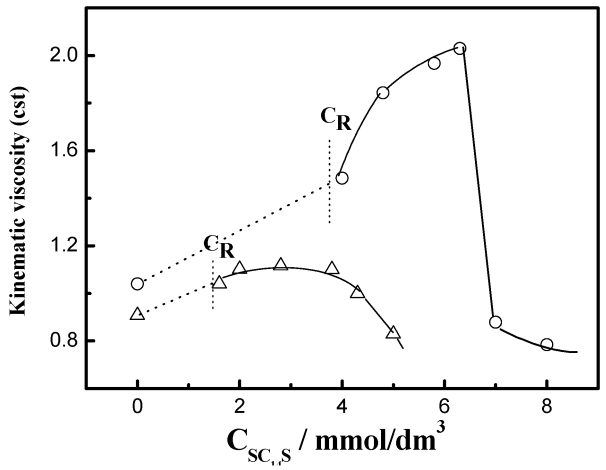

Figure 8. Kinematic viscosity of D40OCT30−$SC_{14}S$ mixtures after redissolution, at polymer concentrations of (△) 0.10% and (○) 0.25%.

Therefore, the observed enthalpy curve tends to the one observed in the absence of polymer. The C_M and the corresponding ΔH_M are also listed in Table 2.

The observed enthalpy curves for D40OCT30/SC_8S systems present a different pattern. A key distinction is that no break corresponding to $CAC_{complex}$ appears, such as that detected for $SC_{12}S$ and $SC_{14}S$. Since SC_8S is a surfactant with a very large cmc (138 mmol/dm^3), it is impossible to form cross-linking mixed micelles of SC_8S with the side groups of the polymer before cnc, although the surfactant is interacting with the charged sites of the polymer chain by electrostatic interaction. Here the SC_8S molecules neutralize the charges of the polymer and the hydrophobicity of the D40OCT30−SC_8S complex increases with the addition of surfactant. This promotes the precipitation of the D40OCT30−SC_8S complex at a much lower concentration (C_P) than the cmc of the pure surfactant (Figure 5). The occurrence of precipitation at this point was confirmed by turbidity measurements (Figure 5b). This will be further discussed when we describe the proposed mechanism of interaction in detail. When the surfactant concentration reaches C_S ($n_{SC_8S}/n_{\text{side group}} \approx 1.3$), all charged sites of the polymer have bound SC_8S molecules. After C_S the pattern is similar to the dilution of pure SC_8S. In the low concentration region experiments the precipitate formed is not dissolved at the end of the titration (Figure 5). For the high concentration region (Figure 6), we should note that the curves for the lower polymer concentrations (0.10 and 0.25%) are very similar to the pure surfactant curve. Only for 1.0 and 3.0% do the curves start to significantly deviate from pure surfactant, but they still have a similar tendency.

Kinematic Viscosity in D40OCT30−STS Mixed Solutions. The surfactants substantially alter the rheology of polymer solutions. The interactions of HMPE with an oppositely charged surfactant often give rise to two maxima in viscosity, before and after the two-phase region. Such behavior is dependent on surfactant concentration and different types of intra-or intermolecular interactions in the system.[10]

Kinematic viscosity measurements have been made as a function of the surfactant concentration on D40OCT30 (0.10% or 0.25%)−$SC_{14}S$ systems (Figure 8). The results show that the kinematic viscosity starts to increase with increasing surfactant concentration at redissolution concentration (C_R) and the system presents gel morphology. This point was exactly the one where we observed by calorimetry a large increase in heat of friction that we interpret as resulting from an increase in viscosity. The kinematic viscosity results confirm our calori-

TABLE 2: Critical Concentrations for Aggregation and Micellization and Enthalpy of Micellization for D40OCT30/SC$_n$S

	$CAC_{complex}$ (mmol/dm^3)	C_M (mmol/dm^3)		ΔH_M (kJ/mol)	
$C_{polymer}$ (w/v %)	$SC_{14}S$	$SC_{14}S$	SC_8S	$SC_{14}S$	SC_8S
0.05	0.48	2.43		−4.2	
0.10	0.79	3.02	139	−2.2	−2.13
0.25	2.15	6.30	140		−2.06
1.0			159		−1.9
3.0			212		−0.85

metric findings. After a maximum the viscosity starts to decrease, reaching eventually a value that is lower than the observed one in the absence of surfactant. At sufficiently high surfactant concentration the excess of free surfactant molecules increases very much the ionic strength of the solution, and that strongly reduces the viscosity of a polyelectrolyte solution.

Phase Behavior in D40OCT30/SC$_n$S Mixed Solutions. We have characterized the events that take place at varying polyelectrolyte/surfactant ratios by combining the ITC results with the turbidity and kinematic viscosity measurements. Figure 9 shows the 3-D diagram with phase separation lines of mixtures

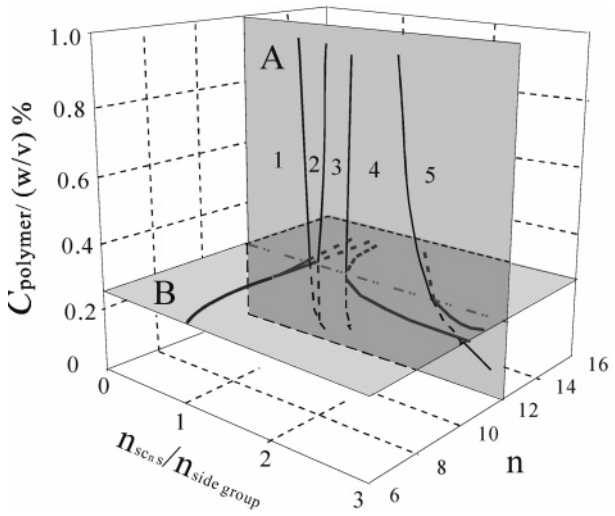

Figure 9. The 3-D diagram with phase boundaries of mixtures of D40OCT30 and SC$_n$S. The regions 1−5 are present in plane *A* and in *B*, and they represent the following: 1, solution of D40OCT30−SC$_n$S complex; 2, cross-linking mixed micelle solution with positive net charges; 3, precipitation and a solution; 4, gel of pseudosingle phase; 5, surfactant-rich mixed micelle and/or free surfactant micelle.

of the polymer and the different anionic surfactants. We have two upright cross sections: plane *A* is set at a fixed number of CH_2 groups in the surfactant alkyl chain ($n = 12$) and represents $C_{polymer}$ vs $n_{SC_nS}/n_{side\ group}$; plane *B* is set at a fixed polymer concentration, namely $C_{polymer} = 0.25\%$, and therefore represents n vs $n_{SC_nS}/n_{side\ group}$. In plane *B* we can see the relationship between alkyl chain length with even carbon number and phase behavior of the mixed systems. The regions from 1 to 5 are present in plane *A* and in *B*, and they represent the following: 1, solution of the D40OCT30−SC$_n$S complex ($C < CAC_{complex}$); 2, solution of cross-linking mixed micelle formed by ion pairs of surfactant and polymer side chain ($CAC_{complex} < C < C_P$); 3, a two-phase region with precipitate and solution ($C_P < C < C_R$); 4, gel phase ($C_R < C < C_M$); 5, solution of surfactant-rich mixed micelle and free surfactant micelle ($C > C_M$). The molar ratio corresponding to $CAC_{complex}$, the boundary between phases 1 and 2, decreases slightly with the increase in $C_{polymer}$ (the approximate mean values of $n_{SC_nS}/n_{side\ group}$ are 0.7 for $SC_{14}S$ and 0.8 for $SC_{12}S$). The molar ratios corresponding to C_p are independent of $C_{polymer}$; i.e., the boundary between phases 2 and 3 for $SC_{12}S$ and $SC_{14}S$ is $n_{SC_nS}/n_{side\ group} \approx 0.9$. For SC_8S no phase 2 is found, and the boundary between phases 1 and 3 is $n_{SC_nS}/n_{side\ group} \approx 0.8$. For the redisolution curve, the molar ratio between phases 3 and 4 also is almost independent of $C_{polymer}$ for $SC_{12}S$ and $SC_{14}S$ ($n_{SC_nS}/n_{side\ group} \approx 1.4$ for $SC_{12}S$ and 1.3 for $SC_{14}S$), but changes with $C_{polymer}$ for SC_8S (shown in Figure 10). The molar ratio corresponding to the formation of phase 5

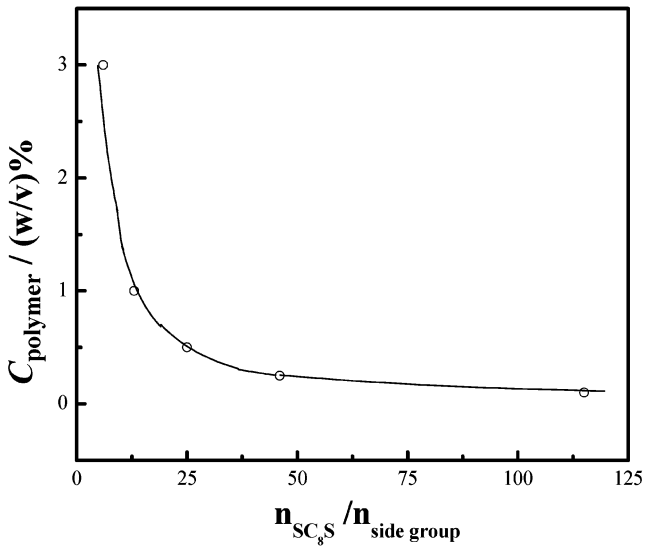

Figure 10. $C_{polymer}$ vs $n_{SC_8S}/n_{side\ group}$ for D40OCT30/SC_8S systems. The $n_{SC_8S}/n_{side\ group}$ values correspond to C_M value for each studied polymer concentration.

changes largely with $C_{polymer}$ and n. For the D40OCT30/SC_8S system, it is noted that the C_R and C_M values (Figure 6) are the same. In Figure 10 we can see the plot of $C_{polymer}$ values against $n_{SC_8S}/n_{side\ group}$ for the D40OCT30/SC_8S system, where C_M values (Table 2) will appear at lower $n_{SC_nS}/n_{side\ group}$ values as $C_{polymer}$ increases. When $C_{polymer}$ changes from 0.10% to 3.0%, $n_{SC_nS}/n_{side\ group}$ at C_M changes from 115 to 6. In comparison with the aggregation number of pure SC_8S in aqueous solution (Table 1), we can see that for $C_{polymer} = 0.10\%$ the exceeding surfactant molecules are enough to form free micelles, but for $C_{polymer} = 3.0\%$ they are not. Therefore, at this polymer concentration the surfactant molecules self-associate into mixed micelles with the polymer pendant groups.

Mechanism of Interaction between D40OCT30 and SC$_n$S. From the above analysis of the results obtained from ITC, supported by turbidity and kinematic viscosity measurements, a more complete picture of the interaction mechanism for the studied D40OCT30/SC$_n$S systems emerges, unraveling the details of the effect of surfactant alkyl chain length on PES interactions.

1. D40OCT30 Self-Assembly. The structure of D40OCT30 is similar to a polysurfactant connected with hydrophilic spacers at the level of headgroups (Figure 11a). Therefore, the hydrophobic tails can self-assemble to form aggregates. Previously[28] we have identified for this polymer a cmc of 0.006%, at which

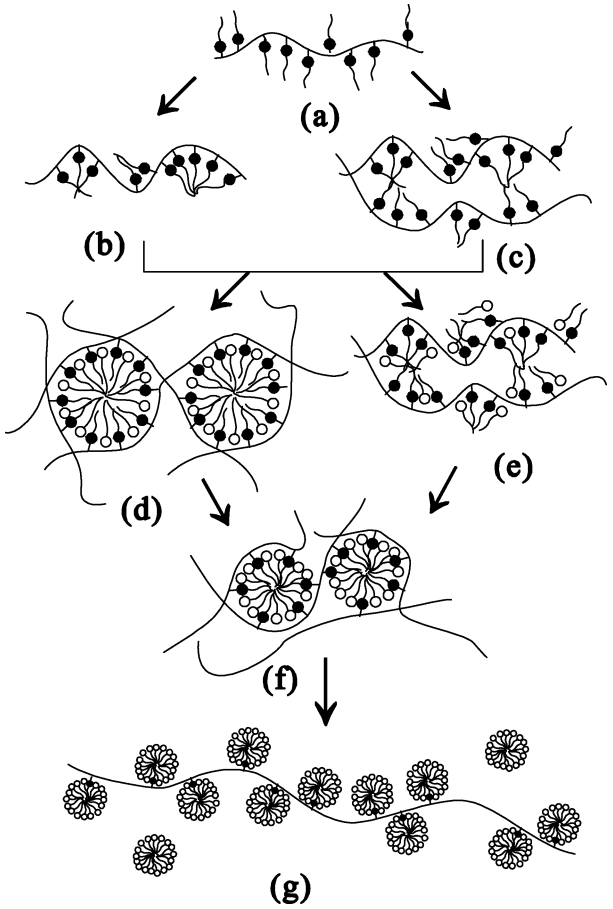

Figure 11. Illustration of interaction mechanism for D40OCT30/SC_nS systems. (●) denotes positively charged group and (○) denotes negatively charged group. (a−c) D40OCT30 solution in the absence of surfactants; (d) cross-linking mixed aggregates for $n = 12$ and 14 formed as the concentration of surfactant is between $CAC_{complex}$ and C_P; (e) mixed hydrophobic clusters for $n = 8$ formed as the concentration of surfactant is below C_P; (f) surfactant-rich mixed aggregates with negative net charges formed after redissolution; (g) surfactant molecules self-associate into micelles in the presence of polymer ($C(SC_nS) \gg C_M$).

the pendant groups self-assemble to form intramolecular micelle-like clusters (Figure 11b). Considering the moderate flexibility of the backbone and the short side chain of the polymer, it is to be expected that the aggregation number of these clusters is very small. With ITC a second break (>0.1%) was determined, corresponding to intermolecular clusters partly obtained by hydrophobic cross-linking (Figure 11c). Both aggregate morphologies will affect the interaction energy of polyelectrolyte and surfactant, but will not give rise to a different interaction mechanism.

2. Formation of Cross-Linking Mixed Aggregates. For D40OCT30/$SC_{14}S$ and D40OCT30/$SC_{12}S$ systems, as discussed above, at $CAC_{complex}$ a pronounced break indicates the formation of cross-linking aggregates with positive net charges. The $CAC_{complex}$ (see Table 2) may be smaller or larger than the cmc of the surfactant, depending on the concentration of the polymer. It is well-known that, in the absence of the polyelectrolyte, the surfactant will form micelles when its concentration is above cmc. However, for D40OCT30/SC_nS mixed systems, surfactant molecules are first attracted to the positively charged sites of the polyelectrolyte by electrostatic interaction, resulting in the formation of pairs composed of a surfactant molecule and a cationic surfactant-like side chain of the polymer. When the surfactant concentration reaches the $CAC_{complex}$, the ionic pairs belonging partly to different backbones and partly to the same one associate into cross-linking aggregates (Figure 11d) by hydrophobic interaction. Therefore, when the concentration of the polymer is higher, a higher surfactant concentration is needed to accomplish the formation of ionic pairs and their subsequent micellization, even higher than the cmc of pure surfactant.

3. Phase Separation. A macroscopic phase separation before cnc is the basic characteristic of the mixed systems of D30OCT40/SC_nS. For the systems with $SC_{12}S$ and $SC_{14}S$, after the formation of the mixed micelle of ion pairs, the second phase appears at $n_{SC_nS}/n_{p-side\ group} \approx 0.9$, whereas for the system with SC_8S it appears at $n_{SC_nS}/n_{p-side\ group} \approx 0.8$. Although the values are similar, we believe that the interaction mechanism is different. We have observed also in another system, D40OCT30/alkylcarboxylate, that for the alkylcarboxylate with a short alkyl chain like sodium acetate no precipitation is observed, even at cnc, whereas with a long chain such as sodium laurate the phase separation takes place, suggesting that the interaction mechanism is dominated by charge neutralization and/or micellization (nonpublished results). In the case of D30OCT40/$SC_{12}S$ or D30OCT40/$SC_{14}S$ the hydrophobic parts of the ion pairs are closed in the hydrophilic shell of the polar groups, due to the formation of mixed micelles before cnc. Further, the mixed micelles are formed with the ion pairs either from the same backbone or from different backbones to avoid excessive curvature of the moderately flexible dextran backbone. Thus the precipitate must consist of the linkage of polymer backbones and has a gel-like morphology. Because the D30OCT40−SC_8S complex does not aggregate into mixed micelles, the added surfactant molecules only incorporate into the clusters (Figure 11e). The hydrophobic part of ion pairs partly exposed to water and the charge neutralization enhance the hydrophobicity of the D30OCT40−SC_8S complex. This could be the reason the precipitation appears at a lower $n_s/n_{side\ group}$ in this case as compared to D30OCT40/$SC_{12}S$ or D30OCT40/$SC_{14}S$ systems. We can therefore conclude that, although charge neutralization is the main reason for precipitation, hydrophobicity also plays an important role.

4. Redissolution and Formation of Surfactant Micelles. For D30OCT40/$SC_{12}S$ or D30OCT40/$SC_{14}S$ after the redissolution concentration (C_R), the mixed aggregates change from electroneutrality to negatively charged (Figure 11f) and the water molecules incorporate into the looser network formed by the D40OCT30−$SC_{14}S$ complex. The gel-like phase which becomes progressively negatively charged swells with water molecules, eventually forming a transparent morphology.[10] Further addition of surfactant makes the aggregates to enlarge and the concentration of free surfactant increases until C_M, where aggregates with less grafted chains of the polymer are formed, and the polymer backbone is stretched because of electrostatic repulsion. After this break (C_M) the observed enthalpy curve tends to the dilution curve of pure $SC_{14}S$, suggesting that a dilution process of $SC_{14}S$ micelles occurs, eventually ($C(SC_nS) \gg C_M$) with a morphology as shown in Figure 11g. The polymer backbone stretches completely, and surfactant micelles are adsorbed to the charged sites of the polymer ("necklace of beads" model).[5,8] The enthalpy change corresponding to this final process decreases with increasing polymer concentration (Table 2), and therefore, at $C_{polymer} = 0.25\%$ we cannot detect any break in the titration curve that would allow determination of C_M (Figure 4). Fortunately, the viscosity measurements (Figure 8) allow the determination of C_M in this case, as for 0.25%; a steep break is found in kinematic viscosity measurements, suggesting that a morphological change takes place ($C_M \approx 6.3$ mmol/dm^3).

For SC_8S at the high concentration region (Figure 6) the curves for the lower polymer concentrations are very similar to the pure surfactant curve, but deviate gradually with the increase in polymer concentration ($C_{polymer} \geq 1.0\%$). After C_M, mixed aggregates are formed and the precipitates start to swell (Figure 11f). After complete dissolution we believe that the final morphology will be similar to the one obtained for $SC_{14}S$ (Figure 11g).

C_M is related to the concentration of the free surfactant in solution, while the value of ΔH_M depends on the aggregation number of the micelle, for each system of the same surfactant and different polymer concentrations (Table 2). C_M increases with polymer concentration as the concentration of free surfactant in the system is smaller at a higher polymer concentration (Table 2). The absolute values of ΔH_M for D40OCT30−$SC_{14}S$ decrease with polymer concentration increase, but in the case of D40OCT30−SC_8S the values of ΔH_M change much less with polymer concentration increase because the mole ratio of surfactant to C_8 grafted chains is much higher (see Figure 10).

Conclusion

We have systematically investigated the thermodynamic characterization of D40OCT30/SC_nS systems. The cmc and the ΔH_{mic} values of SC_nS in the absence of D40OCT30 are obtained from ITC, and their hydrophobic interaction strength is evaluated. Furthermore, in the presence of the polymer, surfactant molecules can strongly associate with D40OCT30 aggregates due to attractive hydrophobic and electrostatic interaction, but interaction characteristics are quite different in D40OCT30/surfactant with a shorter alkyl chain and that with a longer alkyl chain. On the basis of the characterized events that take place at varying polyelectrolyte/surfactant ratios, a 3-D diagram with phase boundaries was drawn for the studied systems, showing the effect of surfactant alkyl chain length on the interaction. The key features are that for SC_8S systems no $CAC_{complex}$ appears and the precipitation occurs in a wide concentration range, but for SC_nS ($n = 12$ and $n = 14$), both precipitation and redissolution occur in a narrow concentration range. A complete mechanism related to the different association processes is proposed.

Acknowledgment. Thanks are due to FCT for financial support to CIQ (UP), Unidade de Investigação 81, for the project SAPIENS 35413/99 and for postdoctoral grants to G.B. and M.N. (SFRH/BPD/5668/2001 and SFRH/BPD/5695/2001).

References and Notes

(1) Hayakawa, K.; Kwak, J. C. T. *J. Phys. Chem.* **1982**, *86*, 3866.
(2) Hayakawa, K.; Kwak, J. C. T. *J. Phys. Chem.* **1983**, *87*, 506.
(3) Malovikova, A.; Hayakawa, K.; Kwak, J. C. T. *J. Phys. Chem.* **1984**, *88*, 1930.
(4) Chu, D.; Thomas, J. K. *J. Am. Chem. Soc.* **1986**, *108*, 6270.
(5) Thalberg, K.; van Stam, J.; Lindblad, C.; Almgren, M.; Lindman, B. *J. Phys. Chem.* **1991**, *95*, 8975.
(6) Thalberg, K.; Lindman, B.; Karlström, G. *J. Phys. Chem.* **1990**, *94*, 4289.
(7) Thalberg, K.; Lindman, B.; Karlström, G. *J. Phys. Chem.* **1991**, *95*, 6004.
(8) Magny, B.; Iliopoulos, I.; Zana, R.; Audebert, R. *Langmuir* **1994**, *10*, 3180.
(9) Petit-Agnely, F.; Iliopoulos, I.; Zana, R. *Langmuir* **2000**, *16*, 9921.
(10) Guillemet, F.; Piculell, L. *J. Phys. Chem. B* **1995**, *99*, 9201.
(11) Kabanov, A. V.; Bronich, T. K.; Kabanov, V. A.; Yu, K.; Eisenberg, A. *J. Am. Chem. Soc.* **1998**, *120*, 9941.
(12) Bronich, T. K.; Ouyang, M.; Kabanov, V. A.; Eisenberg, A.; Szoka, F. C., Jr.; Kabanov, A. V. *J. Am. Chem. Soc.* **2002**, *124*, 11872.
(13) Sokolov, E.; Yeh, F.; Khokhlov, A.; Grinberg, V. Y.; Chu, B. *J. Phys. Chem. B* **1998**, *102*, 7091.
(14) Škerjanc, J.; Kogej, K.; Vesnaver, G. *J. Phys. Chem.* **1988**, *92*, 6382.
(15) Sakai, M.; Satoh, N.; Tsujii, K. *Langmuir* **1995**, *11*, 2493.
(16) Zhou, S.; Hu, H.; Burger, C.; Chu, B. *Macromolecules* **2001**, *34*, 1772.
(17) Zhou, S.; Burger, C.; Chu, B. *J. Phys. Chem. B* **2004**, *108*, 10819.
(18) Monteux, C.; Williams, C. E.; Bergeron, V. *Langmuir* **2004**, *20*, 5367.
(19) Taylor, D. J. F.; Thomas, R. K.; Li, P. X.; Penfold, J. *Langmuir* **2003**, *19*, 3712.
(20) Svensson, A.; Piculell, L.; Cabane, B.; Ilekti, P. *J. Phys. Chem. B* **2002**, *106*, 1013.
(21) Li, Y.; Dubin, P. L.; Havel, H. A.; Edwards, S. L.; Dautzenberg, H. *Macromolecules* **1995**, *11*, 2468.
(22) Hansson, P.; Schneider, S.; Lindman, B. *J. Phys. Chem. B* **2002**, *106*, 9777.
(23) Hansson, P. *Langmuir* **2001**, *17*, 4167.
(24) Konop, A. J.; Colby, R. H. *Langmuir* **1999**, *15*, 58.
(25) Wang, C.; Tam, K. C. *Langmuir* **2002**, *18*, 6484.
(26) Fundin, J.; Hansson, P.; Brown, W.; Lidegran, I. *Macromolecules* **1997**, *30*, 1118.
(27) Claesson, P. M.; Fielden, M. L.; Dedinaite, A.; Brown, W.; Fundin, J. *J. Phys. Chem. B* **1998**, *102*, 1270.
(28) Bai, G.; Santos, L. M. N. B. F.; Nichifor, M.; Lopes, A.; Bastos, M. *J. Phys. Chem. B* **2004**, *108*, 405.
(29) Winnik, M. A.; Bystryak, S. M.; Chassenieux, C.; Strashko, V.; Macdonald, P. M.; Siddiqui, J. *Langmuir* **2000**, *16*, 4495.
(30) Li, Y.; Xu, R.; Couderc, S.; Bloor, D. M.; Warr, J.; Penfold, J.; Holzwarth, J. F.; Wyn-Jones, E. *Langmuir* **2001**, *17*, 5657.
(31) Wang, C.; Tam, K. C.; Jenkins, R. D.; Tan, C. B. *J. Phys. Chem. B* **2003**, *107*, 4667.
(32) Wang, C.; Tam, K. C. *J. Phys. Chem. B* **2004**, *108*, 8976.
(33) Plucktaveesak, N.; Konop, A. J.; Colby, R. H. *J. Phys. Chem. B* **2003**, *107*, 8166.
(34) Anthony, O.; Zana, R. *Langmuir* **1996**, *12*, 1967.
(35) Wang, G.; Olofsson, G. *J. Phys. Chem.* **1995**, *99*, 5588.
(36) Andersson, B.; Olofsson, G. *J. Chem. Soc., Faraday Trans. 1* **1988**, *84* (11), 4087.
(37) Van Os, N. M.; Daane, G. J.; Haandrikman, G. *J. Colloid Interface Sci.* **1991**, *141* (1), 199.
(38) Bijma, K.; Engberts, J. B. F. N.; Blandamer, M. J.; Cullis, P. M.; Last, P. M.; Irlam, K. D.; Soldi, L. G. *J. Chem Soc., Faraday Trans.* **1997**, *93* (8), 1579.
(39) Aniansson, E. A. G.; Wall, S. N.; Almgren, M.; Hoffmann, H.; et al. *J. Phys. Chem.* **1976**, *80*, 905.
(40) Quina, F. H.; Nassar, P. M.; Bonilha, J. B. S.; Bales, B. L. *J. Phys. Chem.* **1995**, *99*, 17028.